

Chapter 5

The quenched narrow-line laser cooling experiments

The extremely narrow transitions found in atoms having two valence electron structure, like the alkaline-earth atoms, can be used to our advantage not only for high-resolution spectroscopy and frequency metrology, but also for atomic cooling. Narrow transitions act as excellent frequency and velocity discriminators, by way of the first-order Doppler shift, and are ideal for some sub-Doppler cooling methods, as I described in Chapter 3. The ability to narrow-line cool Sr and Yb atoms [7, 33, 34] has enabled their use in atomic physics experiments that require trapped atoms with microkelvin temperatures. By implementing a method of *quenched* narrow-line cooling, we extend this cooling method to include atoms with extremely narrow transitions, such as Ca and Mg, whose narrow intercombination lines and correspondingly long decay life times precluded them from direct narrow-line cooling.

In this Chapter I describe the quenched narrow-line laser cooling (QNLC) experiments that we have performed at NIST with ^{40}Ca atoms.[41, 53] Utilizing the results from the Monte Carlo QNLC simulations with the $^1S_0(4s^2) \rightarrow ^3P_1(4s4p)$ intercombination line at 657 nm for cooling and the $^3P_1(4s4p) \rightarrow ^1S_0(4s5s)$ intercombination line at 552 nm for quenching, we first devised and implemented a 1-D step-wise cooling experiment. We then extended QNLC to three dimensions using a method of broadened cooling light and simultaneous application of cooling and quenching light for larger Doppler coverage and improved transfer efficiency. This 3-D, two-color MOT reduced

the atom cloud temperature to $< 9 \mu\text{K}$. With additional third-stage 1-D cooling of this now ultracold cloud of atoms we were able to achieve temperatures of only a few hundred nanokelvin. Resultant ultracold atomic velocity distributions from 1-D second- and third-stage cooling will be compared to our QNLC simulations.

5.1 1-D QNLC experiment

Our first experiments with QNLC were performed in 1-D. This was intended to test the waters of this previously unexplored cooling method and to best utilize the limited available quenching light. Light used to excite the quenching transition was produced by a dye-laser system in the laboratory of Jim Bergquist, also at NIST, that was normally used at 563-nm for use with the Hg^+ optical frequency standard.[48] The light power available for our use was limited to ~ 20 mW by stimulated Brillouin scattering over 180 m of optical fiber that brought the light to the Ca experimental apparatus. To best utilize the available power, a green AOM after the fiber was used as a shutter to control the quenching pulses that excited the atoms. The red cooling light at 657 nm was produced by a diode laser that had been injection locked with light from the master ECDL system, as described in Chapter 4. For cooling, the red light was spatially filtered with polarization-maintaining fibers and chopped temporally into cooling pulses that could be directed into the MOT from the opposite directions using two AOMs. For probing, a subsequent pulse of red light was created by one AOM to scan the resultant velocity distributions.

Let us consider the experimental measurement sequence, as shown in Figure 5.1. We began by cooling and trapping the atoms for 7 ms using the broad 423-nm transition, during which time we loaded $\sim 10^7$ atoms from the Ca beam into a blue MOT. This cooled the atoms to 2.4 mK, corresponding to a v_{rms} of 70 cm/s. To avoid large light shifts of the ground state that would compromise the velocity selectivity of the cooling light, we turned off the MOT light for the duration of the second-stage cooling. At

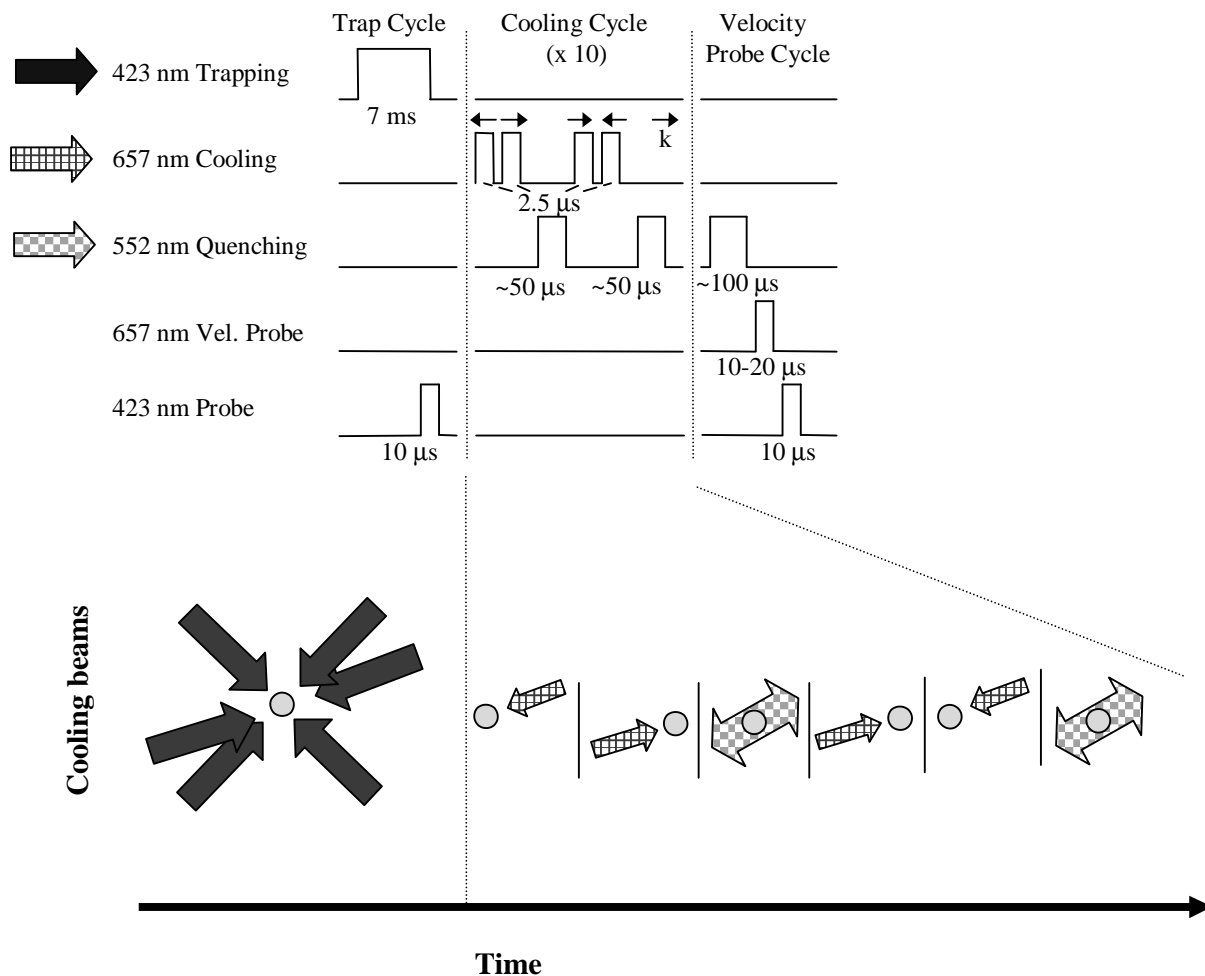


Figure 5.1: Timing diagram for the experimental realization of QNLC. Arrows above the cooling pulses represent the relative direction of the \vec{k} wave vector for each pulse. A laser beam diagram is given below the timing diagram. The frequency of the 657-nm probe pulse is scanned to measure the resulting velocity distributions by making repetitive trapping, cooling and probing cycles. With more quenching power it would be more efficient to use a copropagating 552-nm pulse after each 657-nm pulse, as diagrammed in Figure 3.4.

this point the first blue shelving detection probe pulse was used to measure the total number of atoms in the blue trap.

We then commenced the QNLC with a sequence of counterpropagating red pulses, one from the right followed by one from the left, that were square π -pulses of 2.5- μ s duration, separated by 2 μ s in time. This 657-nm light was spatially filtered with an optical fiber and collimated to a (1/e) diameter of 4 mm with 8 mW in each beam. In order to excite the $m = 0 \rightarrow m = 0$ transition, the light was linearly polarized parallel to the dominant B-field direction, defined by an additional bias field. We detuned the frequency of the red laser ~ 289 kHz to the red of resonance (corresponding to a velocity of 19 cm/s), thus placing the first zero of the sinc^2 excitation lineshape about 110 kHz, or 7 cm/s away from resonance for atoms at rest. After the first pair of red pulses, a quenching pulse was used to pump atoms that had been transferred to the excited state quickly back to the ground state by way of the 1P_1 state. With the green power available, this quenching process takes less than 70 μ s, a time significantly shorter than the 400- μ s decay lifetime of the 3P_1 state. The quenching light intersected the cold atom cloud at an angle of 8° relative to the red cooling beams. As a compromise between cycle time and quenching efficiency, we used a quenching pulse of ~ 50 - μ s duration, with a maximum power of 17 mW (3-mm diameter) standing-wave configuration. These parameters gave about 50 % transfer efficiency of the population from 3P_1 to $^1S_0(4s5s)$. A second pair of red counterpropagating cooling pulses followed the first cooling cycle, but this time in reverse directional order to make the overall cooling process more symmetric (see Figure 5.1), and followed by a standing-wave quenching pulse. This entire cooling cycle was then repeated in order to better transfer the atoms into a colder velocity distribution. After the desired number of cooling cycles, a long green pulse was used to return all the atoms to the ground state. A red probe pulse excited a velocity slice of the atoms resonant with its detuning and a second blue probe pulse read out the excited fraction. For each data point in the final velocity distribution, cooling, probing and detection

was done, and then the red probe detuning was changed for the next data point. This sequence was used to measure the entire velocity distribution (± 3.8 MHz or 250 cm/s) in a total time of 1 s. (Note that this 1-D measurement technique naturally leads us to adopt the convention of quoting 1-D velocities regardless of the dimensionality of the cooling.)

It was important to ensure that the spectral width of our red probe pulses would not significantly add to the measured width of the velocity distribution. To reduce the frequency spread of the pulse spectrum, we needed to make the pulses longer in time, since their frequency coverage goes as the inverse of the probe pulse length. To maintain π -pulse areas for the excitation, we increased the probe pulse length by a factor of 2, and reduced the electric field of the laser pulse by 2, which was accomplished by reducing the red power in the probe beams by a factor of 4. This was repeated until the width of the pulse in frequency was such that continuing to increase the length of the pulse only resulted in a loss of signal-to-noise and no longer reduced the frequency width of the velocity distribution.

The results of these 1-D QNLC experiments can be seen in Figures 5.2 and 5.3. In Figure 5.2, the effect of 15 cooling cycles on the initial distribution is shown, with red cooling pulse lengths of $2.5 \mu\text{s}$ and green quenching pulse lengths of $50 \mu\text{s}$. The QNLC process transferred most of the atoms in the range of ± 30 m/s into the narrow peak at zero velocity, consistent with the expected momentum transfer from the cooling pulses, and from our simulations (dotted line in Figure 5.2.) A Gaussian fit to the central peak yielded a v_{rms} of 6 cm/s, corresponding to a 1-D temperature of $17 \mu\text{K}$. The 14-cm/s width of the central peak in Figure 5.2 resulted from the convolution of the velocity distribution and the frequency spectrum of the $10\text{-}\mu\text{s}$ velocity probe. Data taken at higher probe resolution indicated that that v_{rms} for these conditions is less than 4 cm/s ($7.5 \mu\text{K}$.) The transfer efficiency was estimated by comparing the area of the peak to the area of the initial distribution. In this case we found 30 % transfer, similar to the

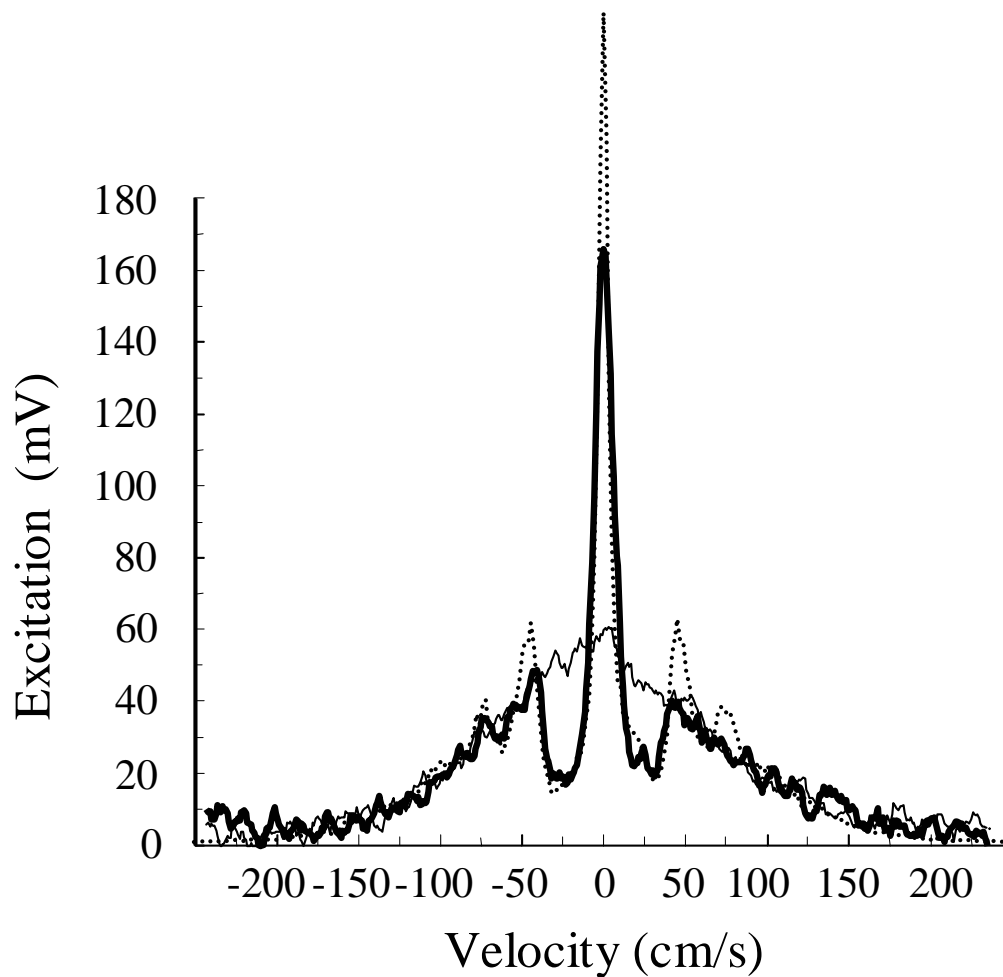


Figure 5.2: Velocity distribution of ^{40}Ca atoms before (thin line) and after (thick line) 15 second-stage cooling cycles. Each cycle consists of two $2.5\text{-}\mu\text{s}$ red pulse pairs each followed by $50\ \mu\text{s}$ of 552-nm quenching light. Finally, a 552-nm light pulse (duration $150\ \mu\text{s}$) is used to pump the remaining excited atoms back to the ground state. The red velocity probe pulse is $10\text{-}\mu\text{s}$ long. The central peak has a $v_{rms} = 5.9\ \text{cm/s}$, corresponding to a temperature of $17\ \mu\text{K}$. This width represents a convolution of the spectral width of the probe and the actual velocity distribution. We are able to transfer about 15 % of the atoms into this cold peak. The dotted line shows a Monte Carlo simulation of the experimental conditions.

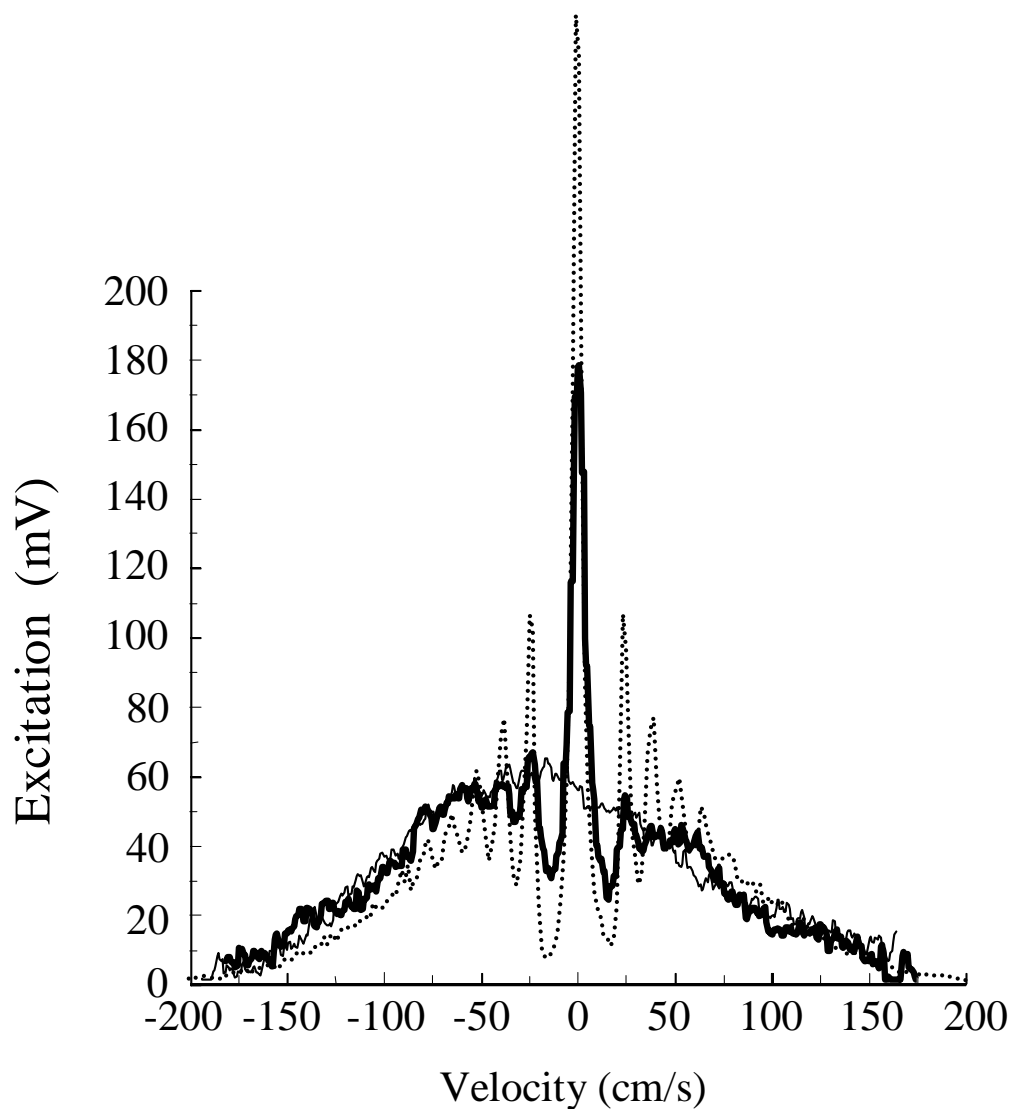


Figure 5.3: Velocity distributions as in Figure 5.2 except using 10 second-stage cooling cycles with increased cooling pulse duration ($5 \mu\text{s}$) and a higher resolution velocity probe ($20\text{-}\mu\text{s}$ duration.) A post-cooling pulse of 552-nm light (duration $100 \mu\text{s}$) is used to pump the remaining excited atoms back to the ground state. The narrow peak has a $v_{rms} = 3.3 \text{ cm/s}$, corresponding to $5.3 \mu\text{K}$. This width represents a convolution of the probe with the actual velocity distribution. The dotted line shows a simulation of the experimental conditions.

value for the simulation. However, since nearly half of the atoms have escaped the interaction region since we first turned off the trapping beams, the net efficiency for this distribution was closer to 15 %, although we have seen transfers as high as 18 %. We believe that fast ballistic expansion due to our warm initial atom cloud temperature (2.4 mK, $v_{rms} \sim 70$ cm/s) has caused the atoms to move into the weaker edges of the laser beams during the cooling and probing periods also reducing the probed atom number. Because of laser power constraints we were unable to increase the beam size, thus the number of cooling cycles we could use was limited to about 15.

When experimentally comparing the use of a small number of cooling cycles to a greater number, we indeed saw increased transfer efficiency and narrower distributions with additional cooling cycles as expected from our simulations. However, during the longer cooling times, more atoms were lost transverse to the cooling direction, limiting the 1-D transfer efficiency. We experimented with using more cooling cycles with less efficient quenching (shorter quenching pulses) and found that the height and breadth of the central peak was fairly insensitive over the range from 18 cycles with 30- μ s quenching time to 8 cycles with 70- μ s quenching time (these values retain the total cooling time ≈ 1.5 ms.)

Striving for colder temperatures, we doubled the length of the cooling pulses to 5 μ s, which made the $sinc^2$ excitation pulse in the frequency domain half as broad, and also adjusted the detuning of the red light to ~ -173 kHz to place the zero of the excitation function closer to zero velocity. To maintain the π -pulse area in this case, we doubled the size of the cooling beams rather than reducing the power in the beams, hoping to increase the pumping efficiency and allow more atoms to stay within the cooling area and be detected. We also used longer red probe pulses to further reduce lineshape broadening.

Figure 5.3 shows the velocity distribution of the atoms after 10 cycles of second-stage cooling with 5- μ s pulses. We indeed saw narrower distributions under these condi-

tions, with a Gaussian fit to the central feature giving a $v_{rms} = 3.3$ cm/s, corresponding to 5.3 μ K. We expected a much smaller fraction of atoms to be transferred to the central peak due to the reduced range of velocities covered by the narrower excitation function, and indeed only about 7 % of the atoms were transferred. Many of the atoms we would like to transfer were caught in other nodes of the sinc^2 lineshape. A simulation of these experimental conditions is shown by the dotted line in Figure 5.3(b).

Two distinct disadvantages plagued these early measurements. The first was the drift of the Fabry-Perot reference cavity used to stabilize the red laser. The cooling light had to be extremely stable with minimal frequency drift in order to remain on resonance with the narrow selected velocity class. The cavity to which the cooling and probe laser were locked drifted at a rate of ~ 30 kHz/minute due to temperature variations in the laboratory. We could reduce this drift to ~ 10 Hz/minute by actively cancelling the drift (feeding a frequency ramp to the 650 MHz AOM) but this cancelled well only on short time scales, which made it difficult to remain on resonance while cooling, affecting the width of the final velocity distribution. By adding heaters to the aluminum box surrounding the cavity and actively controlling its temperature we were able to reduce this drift to < 15 Hz/s, an improvement of a factor of 30. At this rate, it would take about an hour to drift 50 kHz. This improvement allowed us to use a larger number of cooling cycles without the laser drifting during the experiment, leading to narrower measured features in subsequent measurements.

The second problem was that we didn't really have sufficient green power to run as many cooling cycles as needed to cool the atoms to the temperatures we saw were possible from the QNLC simulations. To increase the power of the quenching beams, we installed an argon-ion-pumped dye laser physically closer to the Ca trap. The frequency of this laser was stabilized relative to a hyperfine component of an I_2 transition, nearly coincident with the calcium transition. As the dye laser system was in the lab adjacent to the MOT apparatus, we used 12 m of fiber to transfer the quenching light to the

experiment. This new system incorporated a liquid crystal shutter to control the timing of the quenching pulses. After the fiber and the shutter, ~ 100 mW of light was available for quenching the atoms, and we used a beam 3 mm in diameter (~ 1 W/cm²).

In Figure 5.4 we can immediately see the improvement made possible with the higher quenching power. In this experiment we provided 15 cycles of chirped cooling, with a 50-kHz chirp, meaning that we started the cooling 50 kHz farther detuned than the ideal detuning, and swept it to the ideal detuning over the 15 cycles of cooling time. We continued cooling with the pulse stationary at that detuning for an additional 10 μ s. With the added cooling power we were able to reduce the quenching time to only a few microseconds, and this allowed us to pump nearly all the atoms back to the ground state after each cycle with only 20- μ s quenching pulses, and a final 10- μ s pulse at the end to return all the atoms to the ground state. (These experimental values imply that the in-cooling-cycle quenching pulses could have also been 10 μ s or less.) A 10- μ s red probe pulse was used to read out the velocity, giving a $v_{rms} = 3.4$ cm/s, which corresponds to a temperature of 5.7 μ K. The transfer efficiency was also much greater, with 40 % of the atoms now residing in the narrow peak.

In conclusion, with this method we have been able to reduce the temperature of the ⁴⁰Ca atoms by a factor of 500 using QNLC in one dimension. Atom transfer efficiencies were highest with the chirped cooling and could be enhanced by simply increasing the quenching power to increase the cooling rate. Unfortunately, it is impossible to achieve both large atom number transfers and extremely cold temperatures due to the nature of the *sinc*² excitation lineshape in the simplest single-frequency form of 1-D QNLC. However, the frequency chirping and multiple-pulse/multiple-detuning methods I outlined in Chapter 3 show great potential for higher transfer efficiencies *and* submicrokelvin temperatures.

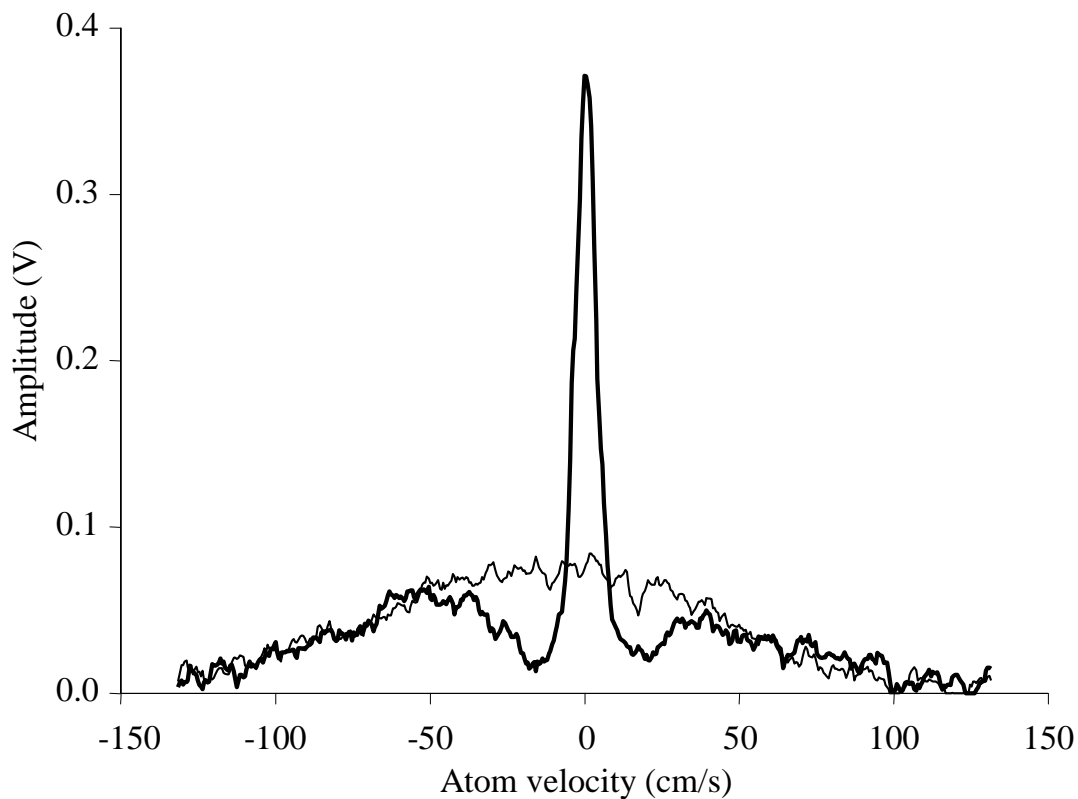


Figure 5.4: Velocity distribution of atoms before and after 15 chirped and 10 stationary 1-D, second-stage cooling cycles. Each cycle consisted of two counterpropagating, temporally separated, $5\text{-}\mu\text{s}$ red cooling pulses followed by $20\ \mu\text{s}$ of $552\ \text{nm}$ quenching light. A $40\text{-}\mu\text{s}$ post-cooling pulse of $552\ \text{nm}$ light was used to pump any remaining excited atoms back to the ground state. The thin line shows the initial millikelvin blue-cooled velocity distribution. Forty percent of these atoms were transferred to the central peak.

5.2 3-D QNLC experiment

Ideally we need an atomic sample cooled in all three dimensions in order to pursue our goal of using these ultracold atoms in our optical frequency standard. As I discussed in Chapter 3, the step-wise excitation method of QNLC can be extended to 3-D, by using a series of pulses incident on the atoms sequentially from all three dimensions. This idea becomes difficult to implement experimentally in 3-D due to issues of laser power and the complications of pulsed beams in all three dimensions. It is more straightforward to implement a cooling approach that could be called quenched Doppler cooling on a narrow transition. This was first demonstrated by Binnewies *et al.* [40] with calcium atoms at PTB. As I described more fully in Chapter 3, this approach uses simultaneous cooling and quenching rather than sequential excitation of the atoms, effectively turning the three-level QNLC system into a simpler two-level Doppler cooling system. In this case the breadth of the cooling transition is equal to an effective transition linewidth, which is approximately equal to the quenching rate and described in Doppler cooling theory.[32] To involve more atoms in the cooling process we also broadened the spectrum of the light used to cool on the narrow transition, as first suggested by Wallis and Ertmer in Reference [35].

For our 3-D QNLC, the cooling light was generated from a stabilized ECDL, whose output was used to injection-lock two more diode lasers, one for the 3-D red trapping beams and the other for the red probe beams. The red trapping light travelled through a polarization-maintaining fiber and was then overlapped with the path of the blue trap beams, with the same $\sigma^+ - \sigma^-$ polarization. The red beams had an intensity of $\sim 20 \text{ mW/cm}^2$ per beam and a $1/e$ diameter of 3 mm. The red trap light was detuned $850 \text{ kHz} \pm 50 \text{ kHz}$ below resonance and broadened to cover a 1.5 MHz wide spectrum by applying frequency modulation at 20 kHz to a 72 MHz AOM. Deviations of 20 % for these modulation parameters did not noticeably affect the cooling results.

To increase the likelihood of absorption of green and red photons from the same direction, thus increasing the cooling force, the quenching beam was given the opposite polarization as the red beams. This increase results from considerations of angular momentum: since the 1S_0 upper state of the quenching transition has only an $m = 0$ level, quenching the $+1$ and -1 m_J levels of the 3P_1 state necessarily requires absorption of σ^- and σ^+ light, respectively. In practice, we found that unless the trapping beams were extraordinarily well overlapped, the green polarization did not greatly affect the final temperature or atom number in the trap, as the beam geometry did not adequately preserve the polarization. Also, to increase the effect of the green light on the atoms and for ease of alignment, the green beam was incident on the atoms in the horizontal plane and in only one of the vertical directions, as shown in Chapter 4, Figure 4.13. We did not see any improvement in the trapping or temperature of the atom cloud when we experimented with a fully 3-D green setup.

To add a spatial component to the second-stage cooling to allow us to also trap the ultracold atoms, we introduced a small magnetic quadrupole field ($\sim 30 \mu\text{T}/\text{cm}$ or $\sim 300 \text{ mG}/\text{cm}$ linear gradient at the center of the trap) during the 3-D quenched cooling. The cooling results were not sensitive to the size of the gradient over the range of $10 - 50 \mu\text{T}/\text{cm}$.

Our method for 3-D cooling followed the timing diagram given in Figure 5.5. We began with first-stage, broad-line, 3-D Doppler cooling on the 423 nm transition, as in the 1-D case, but for a longer time ($\sim 20 \text{ ms}$) in order to increase the initial trapped atom number. We then turned off the 423 nm light and simultaneously turned on the 657 nm cooling light and the 552 nm quenching light for times varying from 1 - 50 ms, at the same time reducing the gradient field from $60 \text{ G}/\text{cm}$ to $300 \text{ mG}/\text{cm}$. The gradient cannot be turned off instantly but rather takes $\sim 1.5 \text{ ms}$ after being turned off to decay to $300 \text{ mG}/\text{cm}$ due to eddy currents induced in the metal MOT apparatus itself. For optimum trapping conditions we would have liked to wait until the field had reached

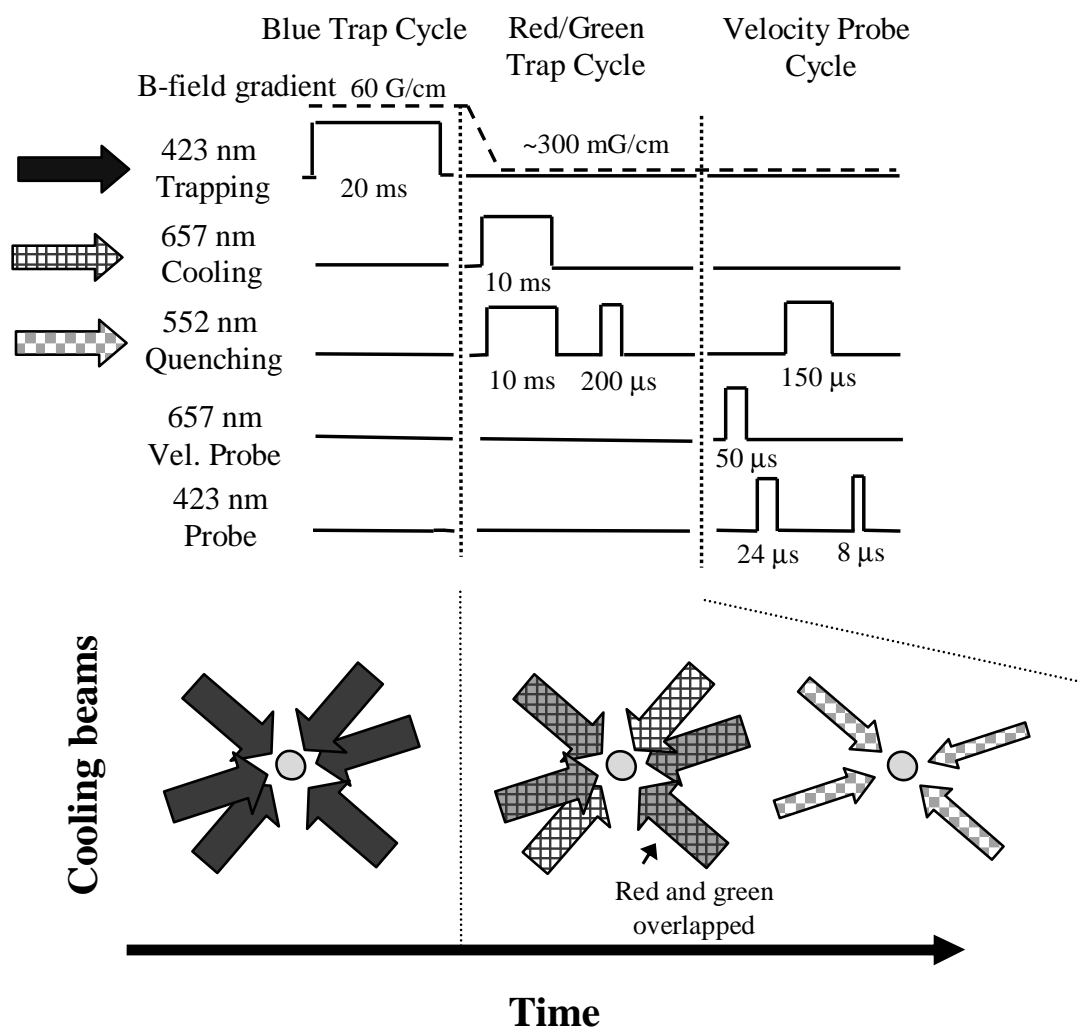


Figure 5.5: Timing diagram for second-stage cooling.

its reduced value before beginning the second-stage cooling cycle. However, this simply lengthened the total cooling time and more effective cooling could be accomplished by turning on the red and green light fields while the magnetic field was decaying. As before, the second-stage cooling was followed by a pulse of quenching light (100 - 200 μs) that was used to transfer the remaining atoms in the excited state to the ground state for maximum detection efficiency. As in our 1-D cooling scheme, the new cold velocity distribution of atoms was probed along one dimension using a red probe beam whose frequency was swept to measure the atom number at one detuning per measurement cycle. To maximize the signal-to-noise ratio, we implemented a novel quenched shelving detection scheme, as described in detail in Chapter 4. In this case, a shelving detection blue probe pulse was applied directly after the red probe pulse, then a quenching pulse of $\sim 200 \mu\text{s}$ returned all the atoms to the ground state. This was then followed by the second blue probe pulse (see Figure 5.5).

Figure 5.6 shows a typical velocity distribution from our first set of second-stage 3-D cooling experiments, where 15 ms of red-green trapping and cooling resulted in a temperature (fit to a gaussian) of $11.5 \mu\text{K}$, giving a $v_{rms} = 4.9 \text{ cm/s}$. As we developed a better understanding of the trapping parameters we were able to achieve the same temperatures in only 5 ms. The symmetry of the measured final velocity distribution was found to be particularly sensitive to the alignment of the retroreflected green cooling beam, since an asymmetry of green absorption leads to an asymmetric force on the atoms. Optimization of the overlap of the retroreflected beams for both the trapping and quenching light increased the atom number and improved the overall symmetry and Gaussian lineshape of the velocity distributions. For this optimization it was quite useful monitor the velocity distributions in all three dimensions and align the trapping beams in each dimension to get the coldest and most symmetric distributions. During this process we were able to ensure that we were cooling efficiently and to the same temperatures in all three dimensions.

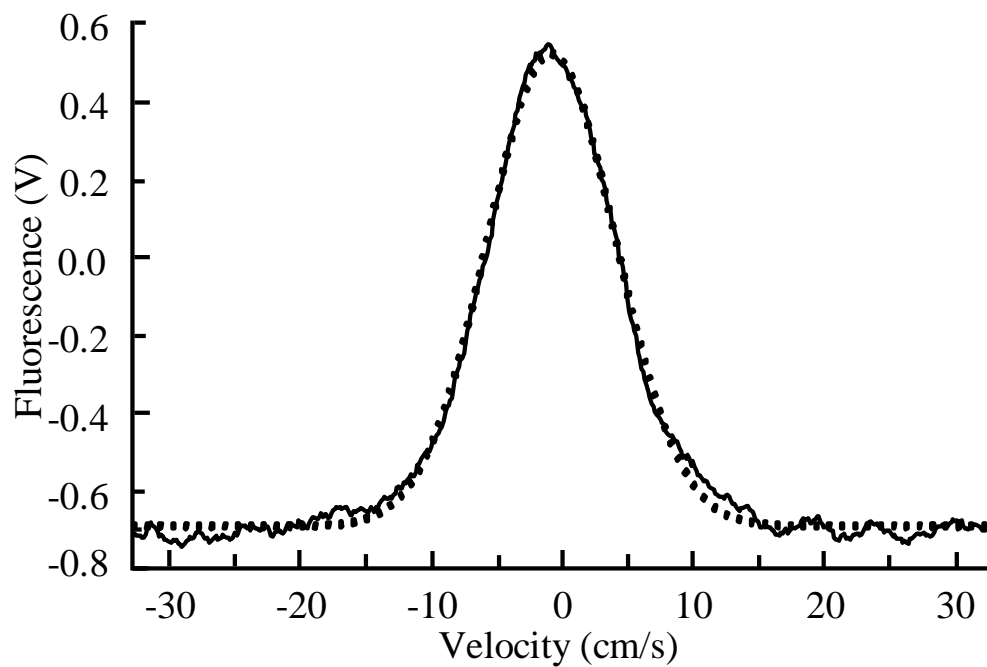


Figure 5.6: Atomic velocity distributions of ^{40}Ca atoms after 15 ms of simultaneous red-green QNLC in three dimensions. A fit to a Gaussian (dotted line) gives an rms velocity of 4.9 cm/s, which corresponds to a temperature of $11.5 \mu\text{K}$.

The number of atoms transferred from the blue trap to the red-green trap decreased with trapping time as shown in Figure 5.7(b). Atom loss comes from two processes. First, in the first 1-3 ms of cooling and trapping, atoms whose velocities were not within the capture range of the red-green trap (~ 40 cm/s) rapidly escaped the observation region. Atoms that were observed after this time were indeed ultracold and trapped, but the measured fluorescence continued to decay, albeit at a much slower decay rate. We believe that the second, slower loss mechanism comes from the fact that the trap itself was not very strong. As atoms moved to the edges of the trap they were perhaps less likely to be quenched, and then were more likely to pick up extra momentum and be pushed out of the trap. The often asymmetric overlap of the red and green trap beams exacerbated this problem. A solution would be to increase the trapping beam diameter. If we had more power in the quenching and cooling beams we could do this without compromising the cooling time.

The temperature of the atom cloud dropped rapidly in the first few milliseconds of red-green simultaneous cooling, and then levelled off below $9 \mu\text{K}$ for longer cooling times, as is shown in Figure 5.7(a). We expect that the lowest temperatures ($\sim 9 \mu\text{K}$) observed for the trapped atoms result from several factors. First, each absorption of a green quenching photon was followed by emission of photons at $1.03 \mu\text{m}$ and 423 nm , which heats the atomic sample by an effective recoil of 3 cm/s , corresponding to a temperature of $4.5 \mu\text{K}$. To eliminate the excess recoil heating, at the end of the second-stage cooling cycle when the atoms have reach a temperature of $10 \mu\text{K}$ or so we could turn off the quenching light and wait for the atoms to decay naturally. This process would add a recoil of only 1.51 cm/s to their velocity, reducing the gain in temperature of the atom by a factor of 4 from that added by the recoils from quenching. Second, since the intensity of the quenching laser determines the effective linewidth of the cooling transition, sufficiently large green power could actually set a lower limit for the temperature. By reducing the green power we could effectively narrow the

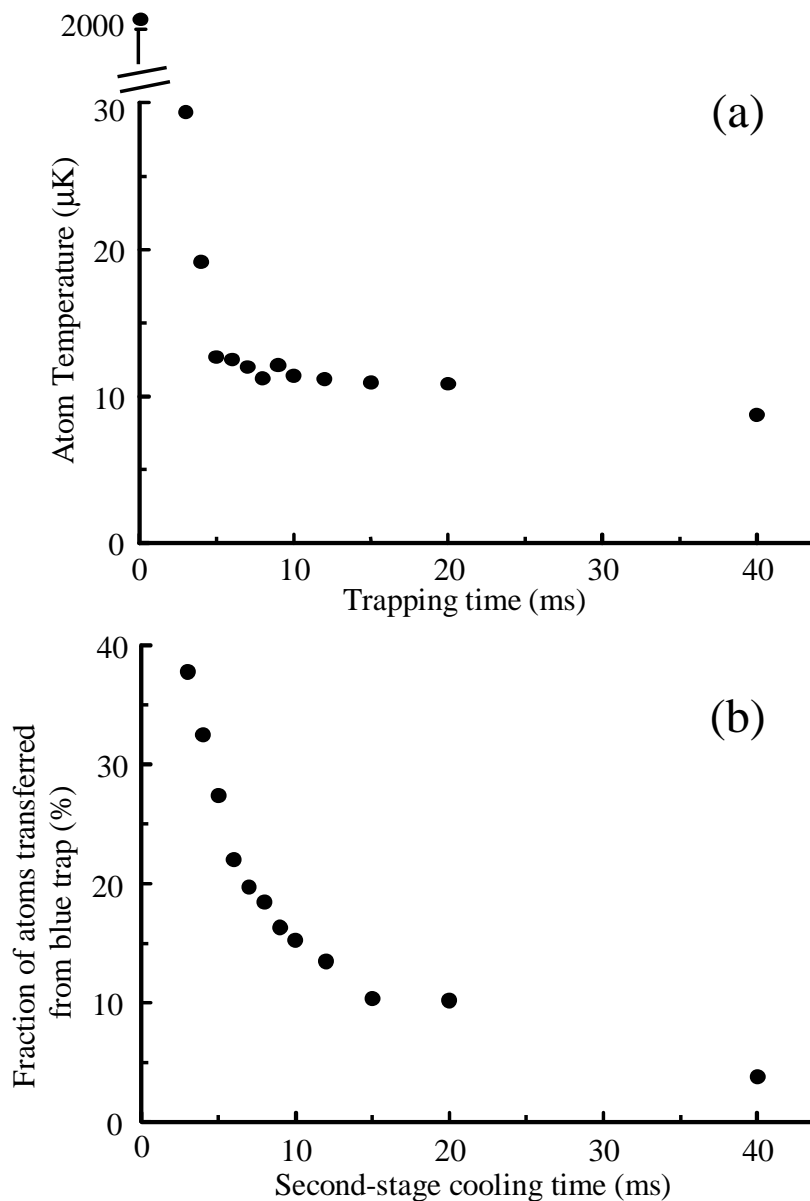


Figure 5.7: (a) Temperature of the atom cloud (corresponding to the rms velocity derived from the fit of a Gaussian lineshape to the measured velocity distribution) vs. second-stage simultaneous red-green cooling time. Measurements of the velocity distribution in the other two dimensions yield similar results. The initial trap temperature with no second-stage cooling is $\sim 2000 \mu\text{K}$. (b) Fraction of atoms transferred from the blue trap to the red-green trap vs. second-stage cooling time.

cooling transition, which would theoretically bring the lower limit of cooling down to the narrow-line Doppler theory cooling limit of $v_{recoil}/2$. Finally, the resultant velocity distributions will be sensitive to the spectrum of the red cooling light (determined here by the modulation depth and detuning) since the spectral distribution contributes to the heating rate of the atoms around zero velocity. We could reduce the modulation depth of the frequency modulation on the cooling light, or change its excitation profile to reduce the width of the final velocity distribution. Another alternative along these same lines would be to return to a pulsed-cooling method at the very end of the cooling cycle in order to create the narrowest lineshapes of all, an idea that I will explore in the next section.

5.3 Additional 1-D QNLC with 10- μ K initial velocity distribution

Starting with a 3-D velocity distribution that is 10 μ K in temperature rather than 2 mK, we revisited our original 1-D pulsed method of quenched cooling in order to attempt to cool and transfer atoms with greater efficiency. We chose to use step-wise excitation instead of simultaneous cooling for this 1-D experiment because it gives much greater control over the frequency spectrum of the cooling light. We used this to our advantage to sculpt extremely narrow velocity distributions and lower temperatures to the 100s of nanokelvin range. Our previous 1-D results had been hindered by two factors associated with the initial millikelvin temperature: the transverse velocity of the atoms set an upper limit of ~ 2.5 ms for the cooling time, while the width of the velocity distribution required many cooling cycles for a majority of the atomic velocity distribution to be transferred to near-zero velocity. With the atoms now starting much closer to zero velocity in all three dimensions, we could hope to reach subrecoil temperatures in one dimension for a nontrivial fraction of the atomic sample.

A typical three-stage cooling cycle is shown in Figure 5.8. We started with the usual blue cooling followed by simultaneous red-green cooling and then added a third

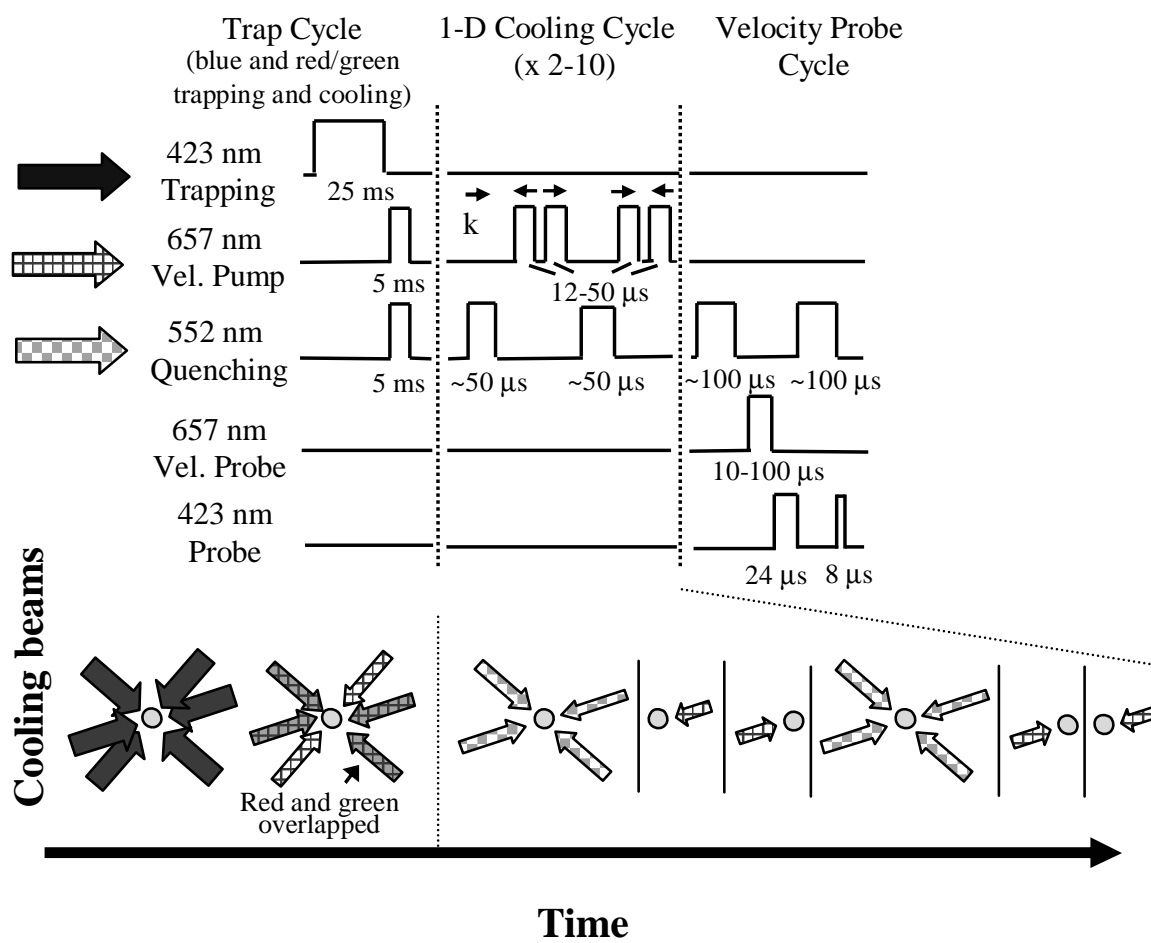


Figure 5.8: Timing diagram for three-stage cooling showing the additional 1-D QNLC

stage of cooling consisting of a series of 657 nm pulses that drive the atomic velocities toward the near-zero excitation region centered at zero velocity. After each pair of sequential red cooling pulses (one from each direction and with an intensity chosen to yield a π -pulse area), a green quenching pulse followed that would send the atoms around to the ground state for another cooling cycle. We alternated the directional order of the red pulses from cycle to cycle to enhance the symmetry of the cooling process. In order to use the $m = 0 \rightarrow m = 0$ magnetic-field-insensitive transition for this third-stage cooling, we used linearly-polarized red light along with a magnetic bias field of 200 μT along the same direction. A third injection-locked diode laser was used for the red cooling and probe pulses, with AOMs controlling the intensity and frequency of the red light. Note that we used the same quenching polarization and spatial configuration as in the second stage so that green light propagated both parallel and perpendicular to the pulsed red light. And as before, we used high-resolution 657 nm velocity probe pulses to measure the final width of the velocity distribution along the direction of the 1-D cooling pulses.

The 1-D velocity distribution that resulted from a series of eight cycles of the third-stage cooling using pulses with 10- μs duration is shown in Figure 5.9. Each cycle contained a quenched red two-pulse sequence followed by another with the red pulse directional order reversed as shown in Figure 5.8.

We found for third-stage cooling with pulses of duration $< 15 \mu\text{s}$ that the velocity distributions fit to Lorentzian lineshapes rather than to the Gaussians, as we found for the case of 3-D cooling. Thus the 1-D results are quoted using half-width half-maximum (HWHM) values of the Lorentzian instead of an rms width.[45] For this sequence of eight cycles, the resulting $v_{(HWHM)}$ of the distribution was 1.3 cm/s, which corresponds to a temperature of 840 nK. For reference, this is approximately equal to the recoil limit for a single red photon. The dotted lines in this figure show two different simulations of the experimental conditions. The lightweight dotted line shows a simulation where

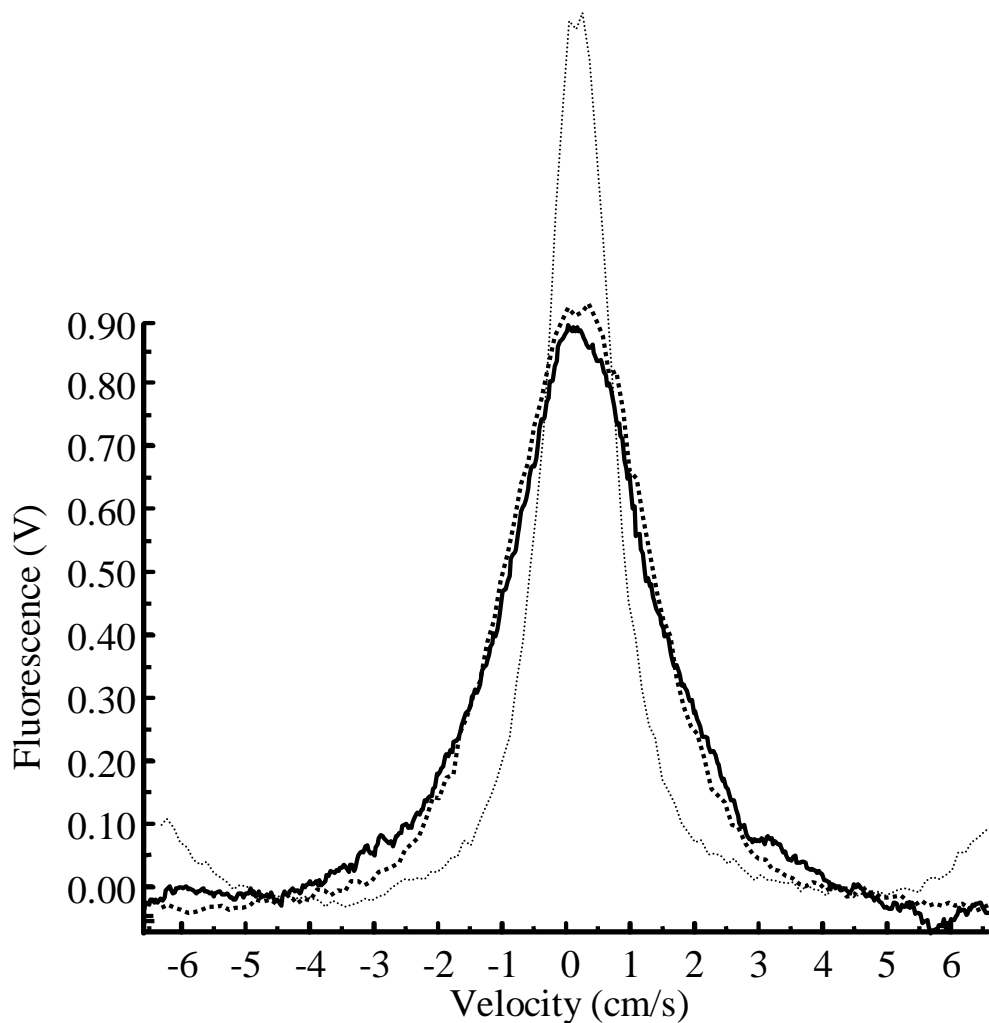


Figure 5.9: Velocity distributions after 6 ms of second-stage cooling followed by 8 cycles of 1-D single-frequency $15\text{-}\mu\text{s}$ red pulses and green quenching. A fit to a Lorentzian yields a velocity (HWHM) of 1.31 cm/s (below the red recoil velocity), which corresponds to a temperature of 840 nK . The lightweight dotted line shows a simulation (same as Figure 3.12) of the experimental conditions, with a detuning chosen to get the coldest distribution. The darker dotted line is a simulation with less than ideal detuning, chosen to match the experimental data.

the detuning (Δ) of the cooling pulses was chosen to create the narrowest distribution, with $\Delta = 3.19$ cm/s. The darker dotted line shows a simulation for which the detuning was chosen to mimic the experimental data, with $\Delta = 4.49$ cm/s. This difference of 1.3 cm/s corresponds to a frequency difference in the cooling laser of only 20 kHz. In simulating this data, I was surprised to find that detuning offsets of as little as 3 kHz could cause drastic changes in the final lineshape if near the critical optimal detuning. This makes it quite difficult to accurately simulate experimental data when using even narrower pulses. It is interesting to note that a majority of the cooling occurred during the first two cycles as was seen in the QNLC simulations, during which time minimal heating of the transverse directions should occur.

As we increased the length of the red cooling pulses beyond 15 μ s in order to reach lower temperatures, additional structure began to appear in the baseline of the velocity distributions as more atoms were trapped in *sinc*² zeros that were not centered at zero velocity. These additional dark states had been seen quite clearly in our previous 1-D experiments and simulations. To reduce this effect, we implemented cooling sequences that used pulses of differing lengths, detuned so as to maximize atom transfer to the zero velocity. In one case we made the first pulse short so that its broad spectrum transferred a large number of atoms towards zero velocity and the second pulse longer so that it produced a narrower velocity distribution. We found that under these conditions, if we allowed the atoms to decay directly from the excited state in order to avoid the extraneous recoils associated with the quenching, fewer atoms escaped the capture/probing region. This, however, had the undesirable consequence of increasing the cooling time by a factor of four. A comparison of distributions showing this effect is shown in Figure 5.10. The solid line shows the results of a sequence consisting of 5 cycles of 15- μ s pulses with 50- μ s quenching pulses, followed by 8 cycles of 25- μ s pulses with 300 μ s of dead time to allow for the natural decay of atoms from the excited state. The dotted line in this figure has the same cooling parameters, but was produced with quenching pulses

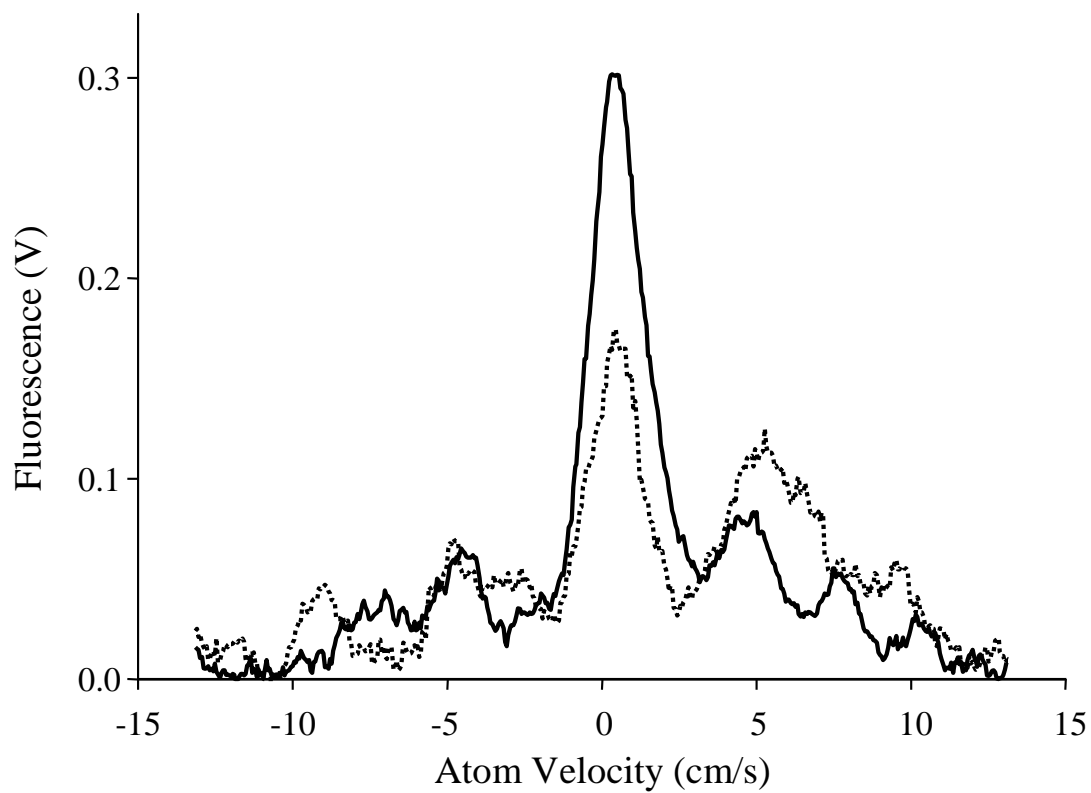


Figure 5.10: Experimental results of a comparison between cooling with quenching pulses after each cooling cycle (dotted line), and cooling where during the last 8 cycles the atoms are instead allowed to decay naturally for $300 \mu\text{s}$ (solid line).

after each pair of red cooling pulses. In Figure 5.11 the experiment with natural decay (solid line) can be compared to a Monte Carlo simulation of this process (dotted line). One can clearly see atoms that have accumulated in small peaks surrounding the other zeroes of the sinc^2 function, now that the detuning and spectral width of the cooling light has been reduced.

Our experiment produced a central feature with a temperature of ~ 520 nK, but as you can see from the comparison of experiment to simulation, there seems to be some offset and asymmetry in the cold peak, most probably due to misalignment of the cooling beams, as we saw in 3-D QNLC. With better alignment, we should be able to realize a much narrower velocity distribution for these experimental parameters. As the cooling pulses are lengthened, the experiment becomes more sensitive to small offsets in the detuning. Using more complicated pulse configurations resulted in complex lineshapes that were not exactly reproduced by the simulations.

In an effort to achieve even colder temperatures we employed a cooling sequence that began with five cycles of $15\text{-}\mu\text{s}$ cooling pulses followed quenching and then by five cycles of $50\text{-}\mu\text{s}$ cooling pulses. For the last five cycles the quenching pulses were not used, and instead the atoms were allowed to decay naturally over a period of $300\ \mu\text{s}$. The resulting velocity distribution (see Figure 5.12) had a temperature of ~ 300 nK with 50 % of the atoms residing in the cold central peak. One can see that a larger number of cycles would help transfer more atoms into this central feature, whose width is only $1/4$ of a single $657\ \text{nm}$ recoil.

A final attempt was made to transfer more atoms into these cold distributions using an alternating pulse method. Instead of performing a number of cycles at one pulse length and then switching to a longer pulse to achieve the coldest distribution, we alternated between short ($15\ \mu\text{s}$) and long ($25\ \mu\text{s}$) cooling pulse cycles. This process produced velocity distributions of just about the same temperature as with the previous method, but as the cooling time increased, loss of atoms began to adversely affect the

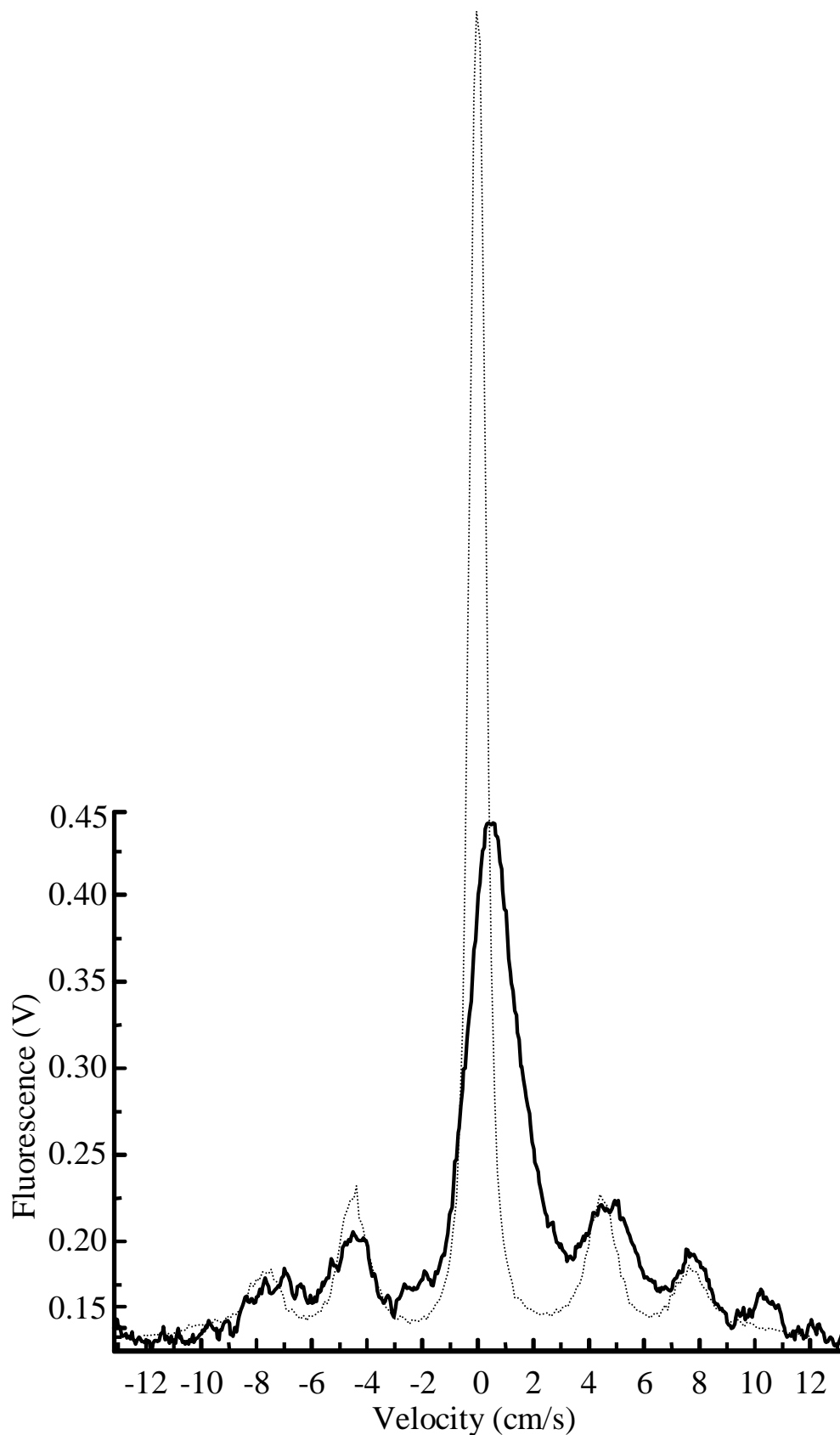


Figure 5.11: Velocity distributions after 5 ms of second-stage cooling followed by 5 cooling cycles with $15\text{-}\mu\text{s}$ red pulses and $50\text{-}\mu\text{s}$ green pulses followed by 8 cooling cycles with $25\text{-}\mu\text{s}$ red pulses and $300\text{ }\mu\text{s}$ of dead time for the natural decay of the atoms from the excited state. A fit of the narrow central feature to a Lorentzian yields a velocity (HWHM) of 1.0 cm/s and a temperature of 520 nK .

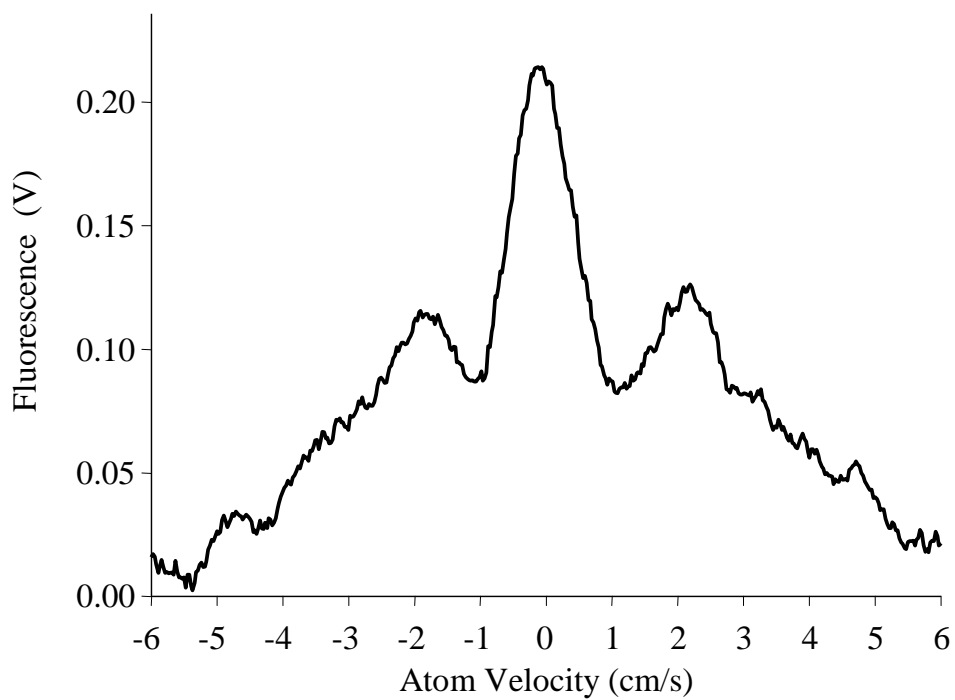


Figure 5.12: Velocity distribution after 5 cycles of cooling with $15\text{-}\mu\text{s}$ red pulses and $50\text{-}\mu\text{s}$ quenching pulses, followed by 5 cooling cycles with $50\text{-}\mu\text{s}$ red pulses and $300\text{ }\mu\text{s}$ for the atoms to decay without quenching. The resultant temperature was the coldest produced experimentally, $T = \sim 300\text{ nK}$.

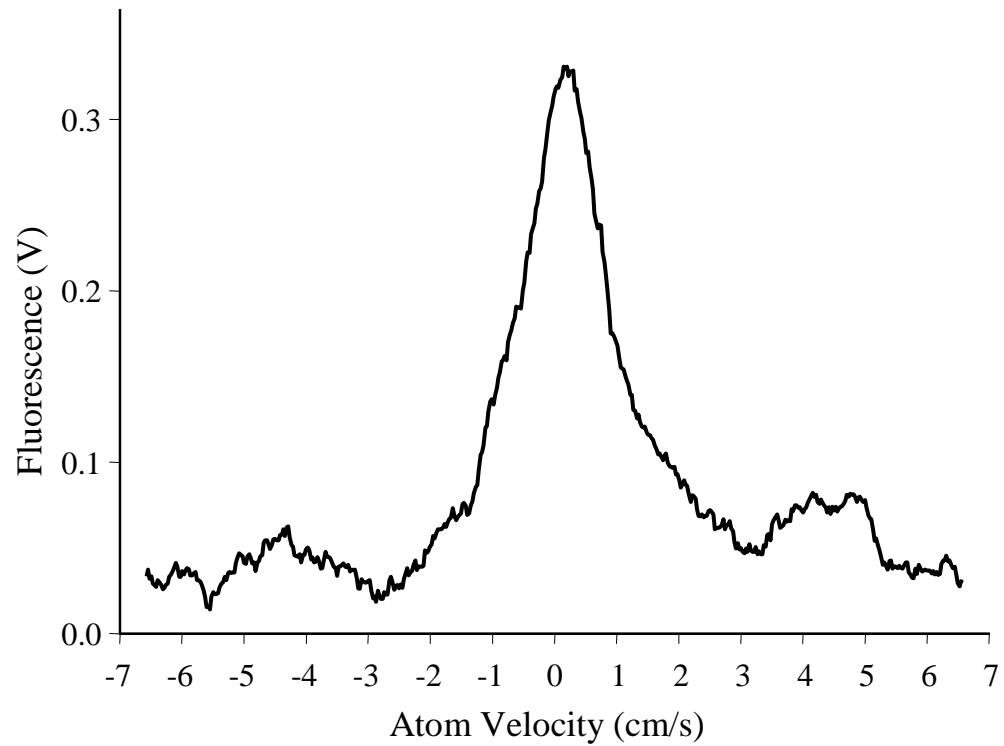


Figure 5.13: Velocity distribution created with the following third-stage cooling cycle: 5 cycles of $15\text{-}\mu\text{s}$ cooling pulses, 5 cycles of $25\text{-}\mu\text{s}$ pulses, then 3 cycles $15\text{-}\mu\text{s}$ cooling pulses followed by 3 cycles of $25\text{-}\mu\text{s}$ pulses. The $15\text{-}\mu\text{s}$ pulses were followed by $50\text{ }\mu\text{s}$ of quenching and the $25\text{ }\mu\text{s}$ pulses were followed by $300\text{ }\mu\text{s}$ of dead time for natural decay.

signal-to-noise of the measurement. A typical result is shown in Figure 5.13.

5.4 Conclusions on QNLC experiments in one and three dimensions

Our MC cooling simulations gave us a great head start in exploring the optimal conditions for QNLC, taking into consideration the initial temperature of the atoms before second- and third-stage cooling and the amount of available quenching light. Using the insight of the simulations we were able to quickly achieve nearly optimal cooling in one dimension with minimal (~ 20 mW) quenching power. Increased quenching power, obtained through the implementation of own dye-laser system increased the number of cooling cycles we could perform, and greatly improve the efficiency of the QNLC.

In three dimensions, simultaneous cooling and quenching allowed us to achieve temperatures of ~ 9 μ K, nearly at the 4 μ K limit set by Doppler cooling theory on this narrow line. Experimental difficulties of aligning a two-color (red-green) MOT had the potential to cause asymmetries in the velocity distribution, but with careful alignment and the ability to measure velocity distributions in all three dimensions, we regularly achieved 10- μ K temperatures all three dimensions in only 5 ms of 3-D QNLC (after 20 ms of blue cooling) with large atom transfer efficiencies. These results are sufficient to utilize these ultracold calcium atoms in our optical frequency standard.

Third-stage 1-D cooling using initially ~ 10 - μ K temperature atoms was shown to reduce the atom temperatures in 1-D to only a few hundred nanokelvin. To reduce the 4.5 cm/s atomic velocity distribution by half, only a few cycles of quenched cooling were needed. With such few decays with randomly directed photon recoils, the other two dimensions would not be heated by more than a few recoils, making such a system quite good for high resolution spectroscopy. In fact, cooling could perhaps be done quickly enough to attempt to use this method to cool the already microkelvin atoms into the nanokelvin range in three dimensions.